Robustness Analysis of Imaging System for Inspection of Laser Beam Melting Systems

Joschka zur Jacobsmühlen*, Stefan Kleszczynski†, Gerd Witt†, Dorit Merhof*
*Institute of Imaging and Computer Vision, RWTH Aachen University, 52056 Aachen, Germany
Email: joschka.jacobsmuehlen@lfb.rwth-aachen.de
†Institute for Product Engineering, University of Duisburg-Essen, Duisburg, Germany

***Abstract*—Laser Beam Melting (LBM) is an additive manufacturing process, which enables the layer-based production of complex parts from metal powder, i.e. "3D printing" with metal. In previous publications, we presented a high-resolution imaging system for inspection of LBM processes, which uses a high-resolution camera to acquire images of each powder layer and laser exposure result. The external camera position necessitates perspective correction, which is based on calibration markers which are "drawn" onto the powder by the LBM system's laser in the first layer. As movements of the powder deposition mechanism cause vibrations, the orientation of the camera may be changed, which would invalidate the calibration results and lead to imprecise measurements or segmentations. To evaluate the effect of these disturbances, we placed calibrations markers in multiple layers and determined the position offset using template matching. We analyze the relative marker drift in three LBM processes and determine the spatial acquisition error. The maximum distance is 4.91 pixels ($156.1\,\mu$m on the part), while most detected markers deviate by less than 1.5 pixels ($46\,\mu$m). Compared to the pixel size of $20\,\mu$m to $32\,\mu$m, these deviations are significant and require a repeated calibration in higher layers for valid high-resolution image-based measurements.**

I. Introduction

Laser Beam Melting (LBM) is a tool-less production process, which iteratively builds a part by producing layers according to 2D slices of the part's geometry. LBM works iteratively: first a thin layer ($20\,\mu$m to $60\,\mu$m) of metal powder is deposited on the build platform, then, the system's laser melts all regions specified by the current layer geometry. This process is repeated, until the entire part is built.

LBM is a very promising technology, but there are still drawbacks, such as missing process documentation and flaw detection [1], [2]. For this reason, we developed an imaging system which acquires layer images of deposited powder layer and laser exposure results [3]. It consists of a high resolution CCD camera with a tilt shift lens, which is mounted to an external mount and monitors the LBM process through the process window (Figure 1). Resulting images were used to categorize common process errors [4] and to detect elevated regions [3], [5], which endanger process stability. Additionally, high resolution layer images enable rating of surface quality, which is correlated with mechanical properties of produced parts [6].

To take full advantage of the obtained data, automated image analysis for contour segmentation, surface inspection and measurements is desirable. Naturally, the precision of image analysis depends on the precision of the image acquisition. In our system, the external position of the camera system introduces perspective distortions, which have to be corrected prior to image analysis. To this end, we use calibration markers, i.e. circles with a perpendicular cross inside, which are created by the LBM system's laser at known positions inside the built layers. By detecting the marker positions in the acquired images, we compute a homography which undistorts the planar quadrilateral for further analysis (Figure 2). This is performed once per process and the result is used to undistort all layer images.

In the LBM process, powder is deposited using a moving powder blade, which accelerates at both ends of the build platform, i.e. vibrations of the camera mount are to be expected. In addition the powder blade may collide with elevated regions of the part causing shocks [5]. In this work, we examine the impact of these effects on the stability and precision of our imaging setup and perform a quantitative evaluation.

II. Method

Our goal is to detect the aforementioned calibration markers in all analyzed layers and to analyze the position deviations to obtain an estimate of the precision of our imaging setup. The following sections describe our approach.

A. Image Data

For analysis, layer images (6576 pixels $\times$ 4384 pixels, image scale $20\,\mu$m/pixel to $31\,\mu$m/pixel) of three LBM processes were acquired using our imaging system. Four calibration markers were placed at the corners of a rectangle in multiple layers of the CAD model starting at the first layer. The marker line width was set to one laser scan line, i.e. $90\,\mu$m. For process (A) markers were built in 250 layers, process (B) contains 249 layer images, and process (C) contains 601 layer images. While the first processes were built without any special preparation, we tightened the camera mount before building process (C) to obtain an estimate of the optimum stability.

B. Marker Detection

Bounding boxes for all four calibration markers were manually defined in the first layer of each process and marker regions were extracted from the first layer image to create

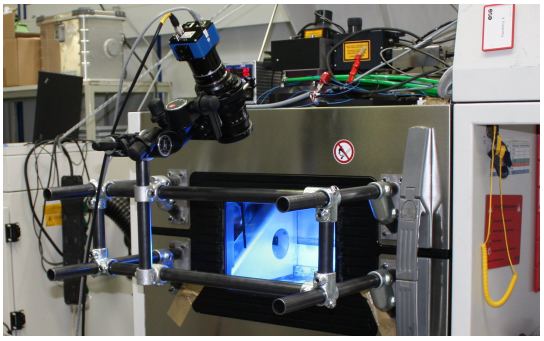

Fig. 1. Camera setup in front of LBM machine. The modular tube construction enables flexible positioning with adjustable height, position, and distance from door. A geared head allows three-axis rotation of camera and camera lens to align it with the build platform.

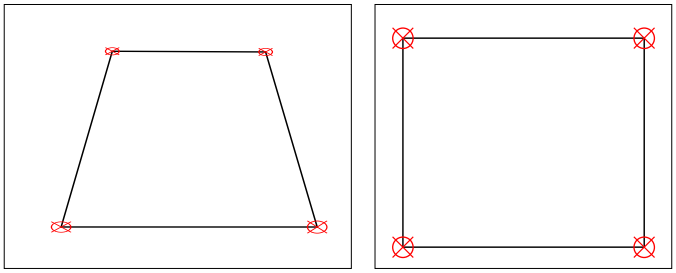

Fig. 2. Perspective Correction. Left: the external position of the camera yields layer images with perspective correction. Using the known position of calibration markers in machine coordinates and their position in the layer image, a homography is computed, which undoes the projective transformation.

templates (Figure 3), which consider the different view angle at the build platform corners.

Calibration marker positions in subsequent layers are detected using normalized correlation-based template matching [7], which is able to deal with changes in brightness or contrast in both analyzed image f and template t. This is achieved by subtracting the corresponding mean intensities and normalizing the correlation coefficient by the variance of the image at the current template position (u, v) and the template variance [7]:

$$\gamma = \frac{\sum_{x,y} \left(f(x,y) - \overline{f}_{u,v}\right)\left(t(x-u, y-v) - \overline{t}\right)}{\sqrt{\sum_{x,y} \left(f(x,y) - \overline{f}_{u,v}\right)^2 \sum_{x,y} \left(t(x-u, y-v) - \overline{t}\right)^2}}, \tag{1}$$

where $\overline{t}$ is the mean value of the template and $\overline{f}_{u,v}$ is the mean value of $f(x, y)$ inside the template t shifted to (u, v):

$$\overline{f}_{u,v} = \frac{1}{N_x N_y} \sum_{x=u}^{u+N_x-1} \sum_{y=v}^{v+N_y-1} f(x,y), \tag{2}$$

for a template of $N_x \times N_y$ pixels. The marker position is then computed as:

$$\boldsymbol{x} = \arg\max \gamma. \tag{3}$$

As our documentation and analysis software was written in Python, we use the open implementation of template matching from [8] in this work.

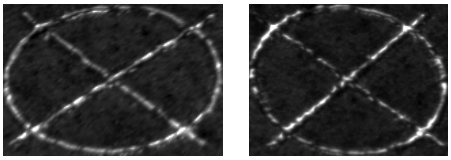

Fig. 3. Example of calibration marker templates. Note, that the original marker is circular, the elliptic form is due to perspective distortion caused by the non-perpendicular view angle. As the distortion depends on the location inside the layer image, separate templates were used for all four markers.

TABLE I
RESULTS OF MARKER DETECTION.

	Distance [pixels]			
Process	Median	75 %-Quantile	Maximum	Pixel Size
A	1.12	1.46	3.16	31.8 µm
B	3.48	3.88	4.91	31.8 µm
C	1.00	1.46	3.82	20.3 µm

To avoid false positive matches and to reduce computation time, marker detection is limited to a search window of 300 pixels × 300 pixels around the reference marker position. As most previously observed deviations are smaller than 10 pixels and the largest marker bounding box measures 237 pixels × 203 pixels this limitation seems reasonable.

To enable subpixel-precise detection beyond the image grid's resolution, template and layer images are scaled by a configurable zoom factor with cubic spline interpolation prior to the matching. The detected position is then divided by the scaling factor to obtain the position in pixels.

C. Drift Analysis

As we are interested in the stability of calibration marker positions inside the layer images, we examine the distance vector of each detected marker to the reference position in the first layer:

$$\boldsymbol{d}_i = \boldsymbol{x}_i - \boldsymbol{x}_{i,0}, \quad i \in 1, \ldots, 4 \tag{4}$$

where $\boldsymbol{x}_{i,0}$ is the marker position in the first layer in image coordinates and i is the marker index for all four positions. We analyze the absolute distances $|\boldsymbol{d}_i|$ by plotting them over the layers' z-position to obtain an estimate of variation with respect to build height. Additionally, distance vectors are displayed in a 2D scatter plot to evaluate the position of detected markers in comparison to the reference marker.

III. Results and Discussion

All quantitative detection results are displayed in Table I. For process (A) the maximum deviation in machine coordinates is 100.5 µm, while Figure 4 shows that most marker distances lie in the range from 0.9 pixels to 1.5 pixels (28.6 µm to 47.7 µm). The position plot in Figure 5 shows that both markers on the right side moved down, while the markers on the left side did not change much and detected positions exhibit only small variation around the origin. This suggests that the camera was rotated around the view axis, which

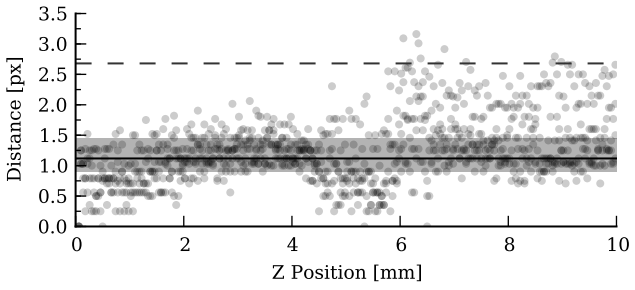

Fig. 4. Distance of calibration markers to start position over 249 layers of process (A), with median distance (–), 25 % to 75 % quantile (■) and the 99 % quantile (- -), which is 2.7 pixels

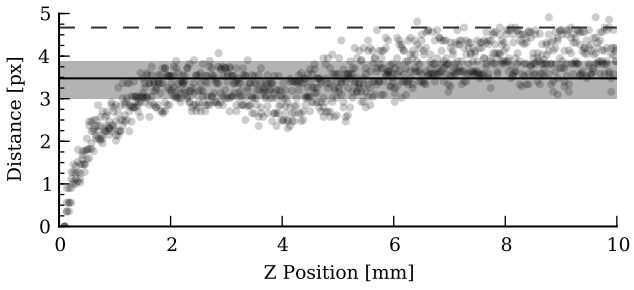

Fig. 6. Distance of calibration markers to start position over 249 layers of process (B) with median distance (–), 25 % to 75 % quantile (■) and the 99 % quantile (- -), which is 4.9 pixels

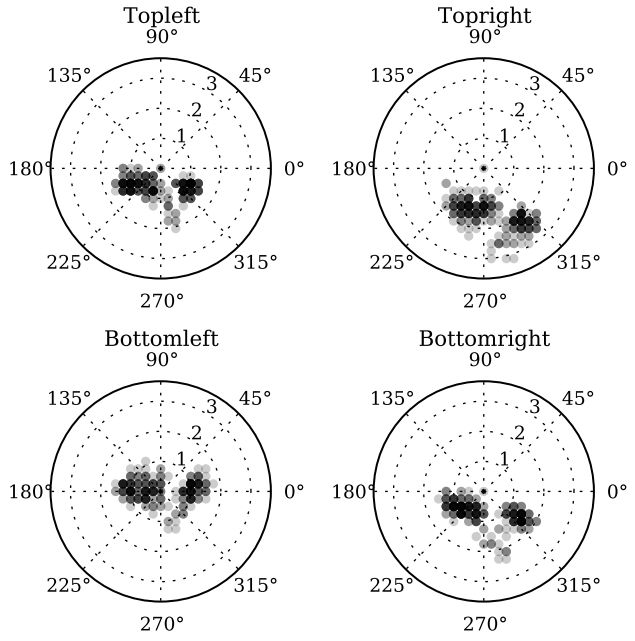

Fig. 5. Positions of detected calibration markers for process (A) (249 layers). Both right markers moved down, which is caused by a slight rotation of the imaging setup.

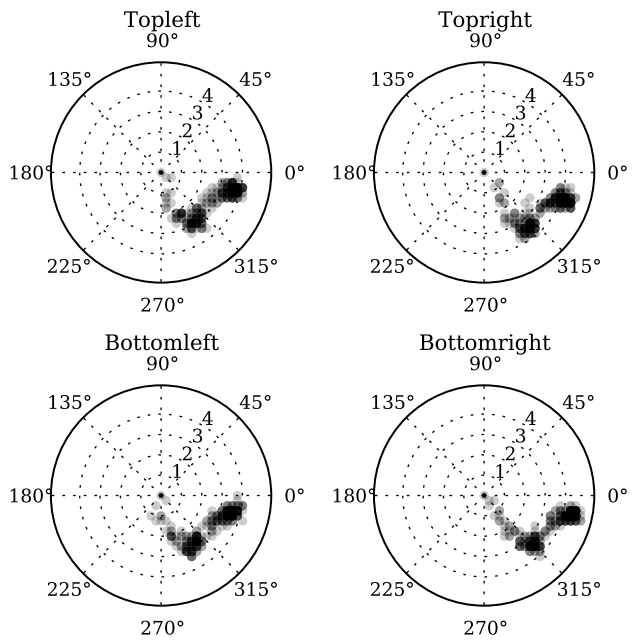

Fig. 7. Positions of detected calibration markers for 249 layers of process (B). Here, the largest deviations are observed and the distributions of all four markers show a similar pattern, which indicates a rigid transformation of the imaging setup, e.g. a slight movement of the entire camera mount.

would complicate a comparison of layer image and reference geometry without proper registration.

For process (B) larger deviations from the reference marker positions are found: the 25 % to 75 %-quantile range comprises distances from 3.01 pixels to 3.88 pixels (95.7 µm to 123.4 µm). Additionally, the distances depend on the z position (Figure 6). Figure 7 shows a movement of all markers down and to the right, with two clusters (darker), which specify two stable locations. This process contained a jewelry part with filigree structures, that collided with the powder blade and caused vibrations, so the marker drift may be caused by a loosened camera mount.

To reduce the impact of vibrations, we explicitly tightened the camera mount for process (C) before the experiment. Now, the median of detected marker distances is 1 pixel and most values lie in the range from 0.7 pixels to 1.5 pixels (14.2 µm to 30.45 µm). Figure 8 shows that larger deviations are present for the first layers, $z < 2.5$ mm, which may be caused by mechanical contact of powder blade and support structures, that are built beneath the part. The distribution of detected positions shows little deviation around the center (Figure 9).

The objective of our work is to provide realistic measurements of the error induced by movements of the imaging setup resolution to consider the impact on reliability and repeatability of image-based measurements. The typical production precision of LBM systems depends on laser spot diameter and part geometry and is around 100 µm [9]. Since measurement best practices call for a measurement precision which is one order of magnitude better than production precision, this can-

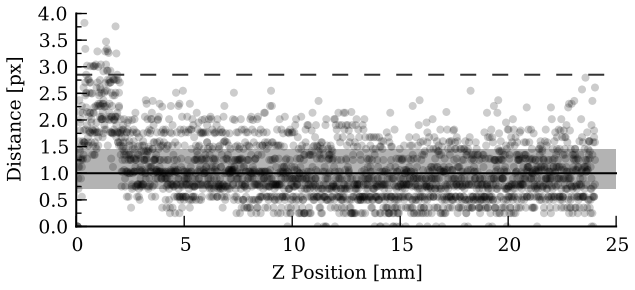

Fig. 8. Distance of calibration markers to start position over 601 layers of process (C) with median distance (–), 25 % to 75 % quantile (■) and the 99 % quantile (- -), which is 2.8 pixels. Larger deviations for $z < 2.5$ mm may have been caused by collisions between coater blade and part during build of the support structures.

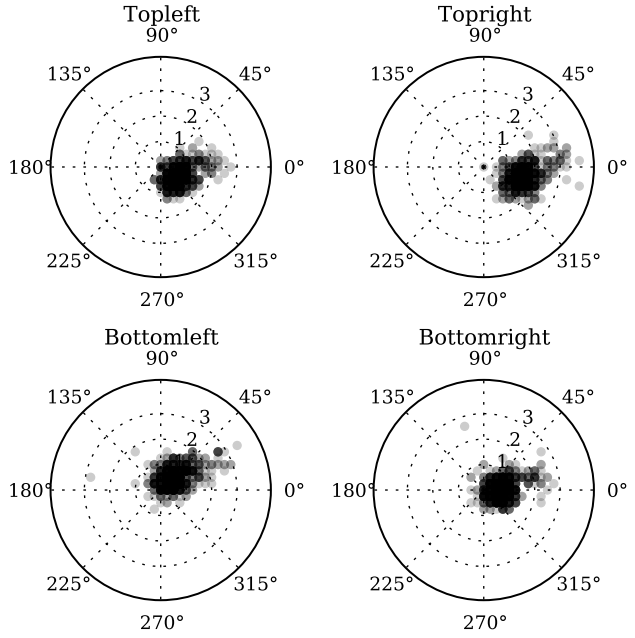

Fig. 9. Positions of detected calibration markers for process (C) (601 layers). Here, the camera mount was tightened before the build process to reduce the impact of vibrations. The position distribution shows less variation and only one cluster: the camera drift did not continue during process acquisition.

not be achieved with our current imaging scale (20 µm/pixel to 32 µm/pixel for the examined processes).

Nevertheless, for best results, the observed effects need to be considered when interpreting the results of image-based measurements for processes with only one calibration (in the first layer). The analysis shows, that optimum results with a precision close to the imaging scale can only be obtained with a repeated calibration which cancels the error caused by the non-rigid imaging setup. Further improving the camera mount does not seem beneficial, as deviations of 46 µm to 156.1 µm are already very small considering the view distance of approximately 0.75 m.

IV. Conclusion

In this work, we examined the stability of our imaging system for inspection of Laser Beam Melting systems to determine the possible variation of spatial measurements in acquired images. We detected calibration markers in 1100 layer images from three different build processes and analyzed the distance between detected marker position in higher layers and the position in the first layer. It was found that the maximum distance is 4.91 pixels (156.1 µm on the part), while most detected markers deviate by less than 1.5 pixels (46 µm). Compared to the pixel size of 20 µm to 32 µm, these deviations are significant and have to be considered when interpreting results of image analysis.

To overcome these errors and to provide high-resolution image-based measurements, calibration of perspective correction has to be repeated in higher layers. The template matching approach presented in this work can be used to track the drift of calibration markers on a sub-pixel scale and correct the detected marker positions. We will integrate these insights into our imaging system to provide a basis for reliable image analysis of part contours and produced surfaces.

References

[1] T. Wohlers, *Wohlers Report 2013. Additive Manufacturing and 3D Printing State of the Industry. Annual Worldwide Progress Report.* Fort Collins, CO, USA: Wohlers Associates, 2013.

[2] J. Gausemeier, N. Echterhoff, M. Kokoschka, and M. Wall, *Thinking ahead the Future of Additive Manufacturing – Future Applications*. Heinz Nixdorf Institute, 2012.

[3] J. zur Jacobsmühlen, S. Kleszczynski, D. Schneider, and G. Witt, "High resolution imaging for inspection of Laser Beam Melting systems," in *IEEE International Instrumentation and Measurement Technology Conference (I2MTC) 2013*, 2013, pp. 707–712.

[4] S. Kleszczynski, J. zur Jacobsmühlen, J. T. Sehrt, and G. Witt, "Error Detection in Laser Beam Melting Systems by High Resolution Imaging," in *Proceedings of the Twenty Third Annual International Solid Freeform Fabrication Symposium*, aug 2012. [Online]. Available: http://utwired.engr.utexas.edu/lff/symposium/proceedingsArchive/pubs/Manuscripts/2012/2012-74-Kleszczynski.pdf

[5] S. Kleszczynski, J. zur Jacobsmühlen, B. Reinarz, J. T. Sehrt, G. Witt, and D. Merhof, "Improving Process Stability of Laser Beam Melting Systems," in *Fraunhofer Direct Digital Manufacturing Conference*, 2014.

[6] S. Kleszczynski, J. zur Jacobsmühlen, J. T. Sehrt, and G. Witt, "Mechanical Properties of Laser Beam Melting Components Depending on Various Process Errors," in *Digital Product and Process Development Systems*, ser. IFIP Advances in Information and Communication Technology, G. L. Kovács and D. Kochan, Eds. Springer Berlin Heidelberg, 2013, vol. 411, pp. 153–166. [Online]. Available: http://dx.doi.org/10.1007/978-3-642-41329-2_16

[7] Briechle and Hanebeck, "Template Matching using Fast Normalized Cross Correlation," *Proceedings of SPIE*, vol. 4387, p. 95, 2001.

[8] S. van der Walt, J. L. Schönberger, J. Nunez-Iglesias, F. Boulogne, J. D. Warner, N. Yager, E. Gouillart, and T. Yu, "scikit-image: image processing in Python," *PeerJ*, vol. 2, p. e453, 6 2014. [Online]. Available: http://dx.doi.org/10.7717/peerj.453

[9] E. Uhlmann, A. Bergmann, P. John, and V. Kashevko, "Verification of Design Rules for Additive Manufacturing," in *Proceedings of the ASPE 2014 Spring Topical Meeting*, 2014.